Nanoscale

PAPER

View Article Online
View Journal | View Issue

Cite this: *Nanoscale*, 2019, **11**, 17920

Surface charged species and electrochemistry of ferroelectric thin films†

Neus Domingo, *‡[a] Iaroslav Gaponenko, *‡[b,c] Kumara Cordero-Edwards, [a,b] Nicolas Stucki,[d] Virginia Pérez-Dieste,[e] Carlos Escudero, [e] Elzbieta Pach, [a,f] Albert Verdaguer [f] and Patrycja Paruch [b]

The combination of scanning probe microscopy and ambient pressure X-ray photoelectron spectroscopy opens up new perspectives for the study of combined surface chemical, electrochemical and electromechanical properties at the nanoscale, providing both nanoscale resolution of physical information and the chemical sensitivity required to identify surface species and bulk ionic composition. In this work, we determine the nature and evolution over time of surface chemical species obtained after water-mediated redox reactions on $Pb(Zr_{0.2},Ti_{0.8})O_3$ thin films with opposite as-grown polarization states. Starting with intrinsically different surface chemical composition on the oppositely polarized films (as a result of their ferroelectric-dominated interaction with environmental water), we identify the reversible and irreversible electrochemical reactions under an external electric field, distinguishing switching and charging events. We find that while reversible ionic displacements upon polarization switching dominate screening in the bulk of the sample, polarization dependent irreversible redox reactions determine surface chemical composition, which reveals itself as a characteristic fingerprint of the ferroelectric polarization switching history.

Received 1st July 2019,
Accepted 2nd September 2019

DOI: 10.1039/c9nr05526f

rsc.li/nanoscale

1. Introduction

Ferroelectric materials showing highly tunable functional responses have become ubiquitous in non-linear optics, memory, electromechanical, and sensor applications. Key aspects of their fundamental properties and performance in devices, such as the structure, stability, and switching dynamics of polarization domains, are driven by electrostatic boundary conditions and determined by the bound charges and associated depolarizing fields at the surfaces orthogonal to the polar axes, as well as by internal screening effects such as band bending.[1–5] In this respect, adsorbed water from the environment has long been recognized as playing a crucial role in electrostatic screening under atmospheric conditions due to its polar nature and ionic conductivity, and the associated screening dynamics have been studied as a function of humidity[6,7] and temperature,[8–10] leading to the development of a full thermodynamic theory of the screening mechanisms.[11] However, few studies and *ab initio* modeling have considered the capacity of water molecules to dissociate and participate in redox chemical reactions at ferroelectric surfaces,[12–16] which would be expected to provide a large additional screening contribution,[17,18] in particular on highly reactive perovskite oxides.[19,20]Moreover, surface chemistry is not only important for the stabilization of ferroelectric surfaces,[21] but in fact polarization switching kinetics are intrinsically coupled to surface electrochemical phenomena.[22–27] Finally, not only the surface but also the bulk chemical composition is susceptible to the polarization direction and switching.[28]

Exploring the coupling between electrochemistry and ferroelectricity is made particularly challenging by not only the spatial but also chemical resolution required, lacking in any one single technique.[29] Scanning probe microscopy (SPM) studies allowing nanoscale resolution and long-duration tracking of ferroelectric domains have demonstrated a difference in surface potential between oppositely polarized domains,[30]

[a]*Catalan Institute of Nanoscience and Nanotechnology (ICN2), CSIC and BIST, Campus UAB, Bellaterra, 08193 Barcelona, Spain. E-mail: neus.domingo@icn2.cat*
[b]*DQMP, University of Geneva, 1211 Geneva, Switzerland. E-mail: iaroslav.gaponenko@unige.ch*
[c]*G. W. Woodruff School of Mechanical Engineering, Georgia Institute of Technology, Atlanta, Georgia, USA*
[d]*University of Applied Sciences Western Switzerland in Geneva (HES-SO/hepia), 1213 Geneva, Switzerland*
[e]*ALBA Synchrotron Light Source, Carrer de la Llum 226, 08290 Cerdanyola del Vallès, Barcelona, Spain*
[f]*Institut de Ciència de Materials de Barcelona (ICMAB), CSIC, Campus UAB, Bellaterra, 08193 Barcelona, Spain*

†Electronic supplementary information (ESI) available. See DOI: 10.1039/C9NR05526F

‡These authors contributed equally to this work.

which moreover evolves with increasing humidity,[6] as well as significant changes in polarization switching dynamics under high humidity (60–70% RH)[22] or liquid immersion.[31,32] These observations point to a dual effect of adsorbed water: it both modifies the spatial distribution of the electric fields generated by a biased SPM tip and plays a key role in polarization screening. They also suggest that polarization orientation strongly influences the interaction of water molecules with the ferroelectric surface.[33–36] Near-ambient pressure X-ray photoelectron spectroscopy (AP-XPS), allowing the contributions of H_2O and OH^- groups to be considered separately,[15,17,37] has corroborated these observations, demonstrating an asymmetric adsorption of the charged species as a function of polarization orientation.[35,36] More recently, the combination of SPM with secondary ion mass spectrometry[38] has suggested that the evolution of chemical states during polarization switching, beside changes in surface chemistry,[39] can also include redistribution of bulk cations.[28,40] However, both the SPM and AP-XPS approaches present some inherent challenges, which can make a fully quantitative analysis of the interaction of water with ferroelectrics difficult.

During piezoresponse force microscopy (PFM) switching studies, the application of a high bias to the tip not only leads to polarization reversal, but also to significant electrochemical effects at the surface.[41] These include the deposition, injection or removal of surface charges,[6,42] as well as structural and chemical changes[43] such as the ordering of vacancies, or even significant surface and sub-surface damage of the sample.[28,41] While many of the electrostatic changes appear to be at least partially reversible, as shown by electrostatic force microscopy (EFM) and Kelvin probe force microscopy (KPFM) measurements of surface charge screening written domains,[6,9,10,22] the chemical effects are not, and obviously influence in their turn the physical properties of the sample. Recent studies have shown that even the simple act of contact scanning with an unbiased tip over a ferroelectric surface can trigger changes, varying from the removal of surface adsorbates and chemical doping of the near surface layer at low contact force,[43] to mechanically induced polarization switching when significant contact forces are exerted *via* strain gradient effects.[44–46] AP-XPS, in contrast, is sensitive to the chemical species and reactions occurring at the ferroelectric surface under water exposure, although at admittedly lower spatial resolution.[47,48] The main challenge of this technique is rather the very restrained humidity range: although called near-ambient, XPS characterization is performed at effective humidity of less than 15% RH,§ obtained through the controlled introduction of water vapor into ultra-high vacuum at room temperature.[37]

For a complete understanding of water adsorption dynamics on ferroelectric surfaces, where it is vital to untangle the effect of the polarization orientation from those of simple charge injection, mechanical scanning effects, and water-mediated surface electrochemistry, the two techniques can be used together. In this work, we present such a comprehensive study of the RH-dependence of the formation and evolution of surface charges on oppositely polarized $Pb(Zr_{0.2},Ti_{0.8})O_3$ (PZT) thin films. AP-XPS measurements show chemical differences in surface adsorbates as a function of polarization orientation, as well as significant changes in both surface adsorbates and bulk ionic distribution between the as-grown state and after polarization switching. We find that while bulk electrochemical changes upon switching can be reversible, the surface chemical composition of the adsorbate layer reveals itself as an imprint of the polarization history of the sample. KPFM measurements tracking the dissipation of surface charge contrast over the full 0–100% RH range[49] confirm that not only the polarization state, but also the sample electromechanical history determines the surface charge dynamics as a function of RH. Thus, by performing the same set of experiments on two oppositely polarized samples one can extract the correlations between the effects of water, applied voltage polarity, contact scanning, and surface charge dynamics, as a function of both the as-grown polarization direction and during polarization switching to better understand the interplay between ferroelectric thin film surface electrochemistry and screening phenomena. Together, these measurements demonstrate the complexity of surface water mediated chemistry and electrochemistry on the surface of ferroelectric oxide thin films, and under dynamic switching conditions.

2. Experimental

The two PZT thin films were both grown by off-axis RF-magnetron sputtering on conductive Nb-doped (0.5% weight) (001)-oriented single crystal $SrTiO_3$ substrates, with the polarization axis therefore out of the plane of the film.[50] The films showed *c*-axis orientation, with no *a*-axis inclusions visible in PFM scans, and no 110 peaks observed during X-ray diffraction characterization. The two films were 100 nm thick and monodomain up-polarized and down-polarized as grown, respectively.

AP-XPS experiments were performed at the NAPP endstation of the CIRCE beamline (BL-24) at the ALBA synchrotron radiation facility, with a photon energy range of 100 eV–2000 eV.[47,48] The total electron energy resolution in the experimental conditions used for the high-resolution spectra is better than 0.3 eV, and the resolution of the XPS spot area is of 30 μm × 100 μm, with good positioning control over the sample surface to locate the beam on selected as-grown or switched polarization areas. Further details about the system can be found elsewhere.[51] Samples were cleaned by heat treatment up to 200 °C over-night in high vacuum conditions ($\approx 10^{-7}$ mbar). The chamber was then evacuated down to $\approx 6.5 \times 10^{-8}$ mbar and the sample cooled down to 21 °C and then water vapor was dosed into the chamber. Water was previously degassed by several freeze–pump–thaw cycles.

§ Higher humidity conditions requires cooling of the sample, but since the magnitude of the polarization itself depends on the temperature, such cooling introduces an additional variable in the experiments, and thus was not considered in the present study.

High-resolution XPS spectra for the Pb 4f, Zr 3p, Ti 2p, O 1s and C 1s core levels were obtained. The fitting of all XPS spectra peaks was performed using the *CasaXPS* software and monolayer coverage for each species was calculated by applying the methodology and the same adsorbates model as previously used for $SrTiO_3$ [15](see ESI† for a detailed description of the fitting methodology).

PM studies were carried out on an *Asylum Research Cypher ES* atomic force microscope with integrated temperature control. Controlled humidity conditions were achieved through the use of a home-built humidity controller with precise, low-noise modulation of RH from 5% to 85%.[49] Conducting PtSi coated tips were used in all measurement cycles (topography imaging, domain writing, KPFM, PFM) for the high stability of their coating. The KPFM measurements were performed in single-pass amplitude modulation mode with an excitation of 3 V*ac* at 5 kHz and proportional and integral PID loop gains of 10 and 5 respectively with topographic feedback in low-amplitude non-contact mode. The typical free oscillation amplitude of the latter was set to a sub-10 nm tip oscillation – reduced to around 5 nm in feedback, in order not to disturb the surface water layer.

To explore the effects of polarization orientation as well as of contact scanning and of the switching history of the sample, we performed parallel humidity-dependent studies on two samples with opposite as-grown polarization orientation, before and after polarization switching. For the AP-XPS experiments, polarization switching was carried out *ex situ* on the as-grown down-polarized sample by applying −10 V to a macroscopic Au electrode patterned on the film surface (Fig. S1†). The electrode was subsequently chemically removed by sonication in organic solvents and the surface and ferroelectric polarization of each area was checked by PFM. Complete Au removal was further probed by XPS analysis on the electrode area. The up-polarized sample was studied only in the as-grown state. For the SPM experiments on the same samples, polarization switching was carried out *in situ*: after RH was stabilized at the target value,[49] the corresponding domain structure was written applying a DC voltage (supercoercive voltages of ±8 V) while scanning the sample in contact mode, and followed using KPFM for up to 12 hours. This sequence was then repeated at increasing humidity values up to ≈80% RH.

3. Results and discussion

3.1. Bulk PZT thin film chemical composition by AP-XPS

AP-XPS measurements in PZT ferroelectric thin films show that the chemical composition close to the surface is strongly correlated to ferroelectric polarization, and moreover, ferroelectric switching under an applied electric field is associated with significant electrochemical effects. XPS gives insight into the chemical composition close to the surface (with an estimated penetration depth of 3 nm for the chosen incident photon energy), and shows differences in the contribution of A and B site cation species in the PZT perovskite structure as a function of polarization. By comparing XPS spectra taken at different incident energy beams (see Fig. 1), it is possible to determine the profile depth distribution of the different ions, and their relative ratio (see Fig. 1d) and thus to extrapolate the relative concentration of the different elements. We observe that as-grown PZT thin films with opposite polarization show an intrinsically different composition close to the surface (see Fig. 1e): as-grown down polarized PZT ferroelectric thin films present a concentration of Ti on the surface more than twice above the nominal Ti/Zr stoichiometry. This result points to a partial substitution of Zr by Ti on the B sites of the negative surface, which can be explained in terms of internal screening mechanisms: the reduced diameter of Ti ions as compared to Zr facilitates the accumulation of oxygen vacancies close to the

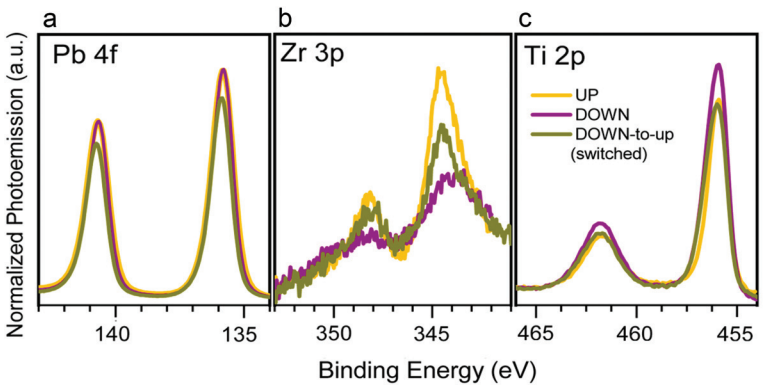

d

Ratio	Ti/Zr	Ti/Pb	
Nominal PZT thin film	4	0.8	0.8
Kinetic Energy	240 eV surface	240 eV surface	560 eV bulk
UP	3,73	1,06	0,77
DOWN	9,29	1,46	0,80
UP switched (as-grown down)	4,21	2,07	1,07

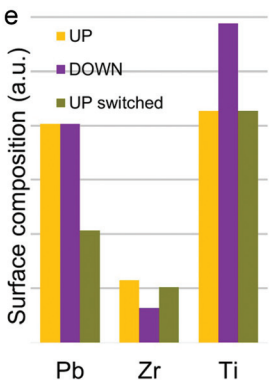

Fig. 1 AP-XPS spectra of the different elements at the (a) Pb 4f edge, (b) Zr 3p edge and (c) Ti 2p edge as a function of ferroelectric polarization state: as-grown up-polarized (yellow), as-grown down-polarized (purple) and down-to-up switched polarization state after the application of a negative bias (green). Spectra in (a), (b) and (c) were obtained at an incident energy of 700 eV and UHV conditions. (d) Ratio of peak intensities of the different metal ions in PZT thin films as a function of the as-grown polarization state and ferroelectric switching with V_{dc} = −10 V. Values obtained for a kinetic energy of 240 eV correspond to a more superficial contribution than those obtained with a kinetic energy of 560 eV, from which it is possible to obtain a depth profile differential contribution. (e) Relative atomic contribution of the three elements to the surface composition of PZT thin films for the polarization states, as depicted from the measured ratios. Down polarized surfaces are characterized by an excess of Ti probably substituting Zr, and switched domains are characterized by a huge increase of Pb vacancies.

surface in agreement with the internal band bending associated with the screening requirements for this surface.[52] Still, the density of oxygen vacancies is very low for our films, and cannot be detected in the Ti edge as Ti^{4+} peaks. Finally, there is an overall decrease of Pb ions, that show less contribution than Ti ions close to the surface, probably associated with the higher volatility of this species in the oxide structure.[53]

Electrically switching this initially down-polarized sample results in: (i) a relative increase of Zr ions close to the surface, as expected for up-polarized domains,[28] (ii) a decrease of Ti ions to the same concentration as that observed on the as-grown up-polarized surface, and (iii) the creation of a big amount of Pb vacancies. While the ionic displacements of Zr and Ti ions upon polarization switching seems to be reversible, the irreversible loss of Pb ions upon electric switching might have strong influence on fatigue effects in ferroelectric thin films.

Our observations are in partial agreement with time-of-flight secondary ion mass spectrometry (ToF-SIMS) analysis of electrochemical changes induced as a result of ferroelectric switching in PZT thin films under a negative tip bias,[28] for which a depletion of Pb^+ and PbO^+ ions was also observed at depths between 2 and 2.5 nm, together with a relative increase of Zr^+ and ZrO^+ content. However, we observe a significant discrepancy with respect to the Ti content enhancement of negative surfaces, for which a possible explanation is the different approach used for polarization switching (macroscopic Au electrode *vs.* nanoscale SPM tip). In summary, from these initial AP-XPS results we can expect that each surface will correspond to intrinsically different chemical perovskite structures and surface terminations as a function of as-grown polarization and switching history: on down-polarized PZT we expect a combination of predominantly PbO and TiO_2 terminations, and on up-polarized surfaces there should be a higher percentage of ZrO_2 terminations.

3.2. Surface PZT thin film chemical composition by AP-XPS

AP-XPS has the required chemical sensitivity to detect water molecules on the ferroelectric surface, whose adsorption and dissociation are well known to depend on the polarization[16,33–36] as well as on surface chemical reactivity,[5,14,16,54] especially for perovskite oxides with TiO_2 terminated surfaces.[15] The total adsorption and the dissociation of water molecules into charged species (–OH groups, protons and peroxide species) is very different as a function of the as-grown sample polarization state. Fig. 2 shows the O 1s spectrum, which can be decomposed into a complex distribution of peaks, assigned to different adsorbate species according to previously reported XPS measurements, as described in the ESI.†[15,36] Spectra of the O 1s region at 1 mbar and 700 eV are shown in Fig. 2 for three different surfaces: up polarized as-grown (Fig. 2a, top), down polarized as-grown(Fig. 2a, middle) and down-to-up polarization switched (Fig. 2a, bottom).

Quantitative analysis of the fittings can be performed using a multilayer electron attenuation model,[15,36] and plotted as a function of RH (Fig. 2b, c and d). Surface hydroxylation shown in Fig. 2b is known to be directly related to surface water dissociation reactions, as a byproduct of water molecules splitting.[55] Once the surface hydroxylation levels are high enough, adsorption of water in a molecular state is favored[15,35,36] (see Fig. 2d). Water appears to have preferential affinity for negative rather than positively polarized surfaces: negative surfaces are more efficient in water splitting resulting in a higher degree of surface hydroxylation already at low RH, which facilitates an earlier formation of surface water monolayers. A correlation between surface hydroxylation and hydrophilicity was also observed for $LiNbO_3$ ferroelectric surfaces,[36] but unlike our results in PZT, it occurred preferentially on positive surfaces. This result suggests that the surface hydroxylation is dominated by the chemical active sites present on the surface and has probably low dependence on the ferroelectric polarization. Moreover, although there are evident reversible bulk ionic displacements of the B site ions of the perovskite structure associated with polarization switching, surface hydroxylation nonetheless shows a strong imprint of the as-grown polarization state: hydroxylation levels do not change after down-to-up polarization switching. All in all this points to the fact that the screening role of both, hydroxyl groups and water molecules is very low, and instead, the hydroxylation state of the surface can be used as a feature revealing the sample polarization history.

In contrast, the coverage of O_{surf}, which we attribute to superoxide species at the surface, appears to respond strongly to the application of electric fields. In particular the application of negative bias to a down-polarized sample leads to a threefold enhancement of these charged species. We note that our recent studies of electrochemistry of TiO_2 based surfaces in a water environment[15] demonstrated that radiation promotes surface redox reactions, observed as an increase of the species contributing to the O_{surf} peak. We expect that the application of negative voltages to the surface, besides polarization switching and electronic charge injection, can likewise lead to similar redox electrochemistry of the ferroelectric surface. In this case, for a highly hydroxylated surface, a possible reduction will be $4\ –OH + 4e^- \rightarrow 2O^{2-} + 2{\cdot}H_2O$, leading to the observed increase in the O_{surf} and molecular adsorbed water peaks. Finally, probably as a result of both maintaining the hydroxylation state and the strong enhancement of the oxidized species, we observe that the water adsorption rate is clearly maximized for the down-to-up switched polarization state, leading to the following scaling for surface hydrophilicity: $P_{\text{down-to-upswitched}} > P_{\text{down}} > P_{\text{up}}$.

XPS can also be used to evaluate the electronic diffusivity of ferroelectric surfaces as a function of RH by measuring the energy shift of XPS spectra with respect to expected values for non-charged surfaces.[36,56] Fig. S2† shows the evolution of the kinetic energy shift of the oxide peak from the O 1s spectra, which is sensitive to surface charge effects under XPS irradiation and stray fields. It is well-known that the main path for surface discharge in this type of experiments is the formation of a full monolayer of water which triggers the onset of surface electronic and ionic conductivity.[36] In this case, we

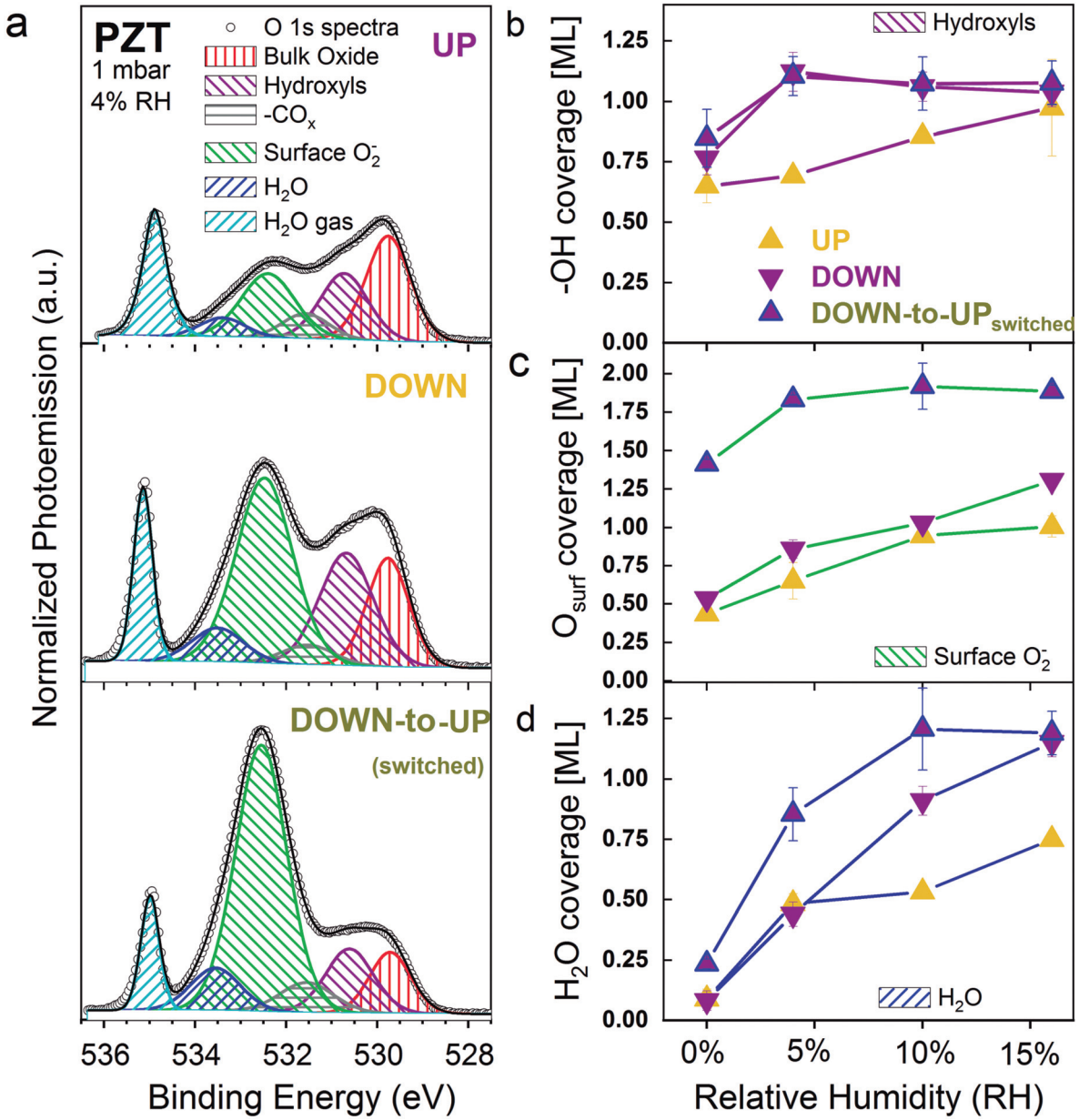

Fig. 2 (a) Normalized photoemission of the O 1s range spectra taken at an incident energy of 700 eV and 1 mbar of H_2O pressure at room temperature for the as-grown up-polarized (left column – top), as-grown down-polarized (left column – middle) and down-to-up switched (left column – bottom) states. Spectra are decomposed into 6 different peaks depicting the contributions from different oxygen-based species as explained in the text. The right column shows the calculated coverage in monolayers of 3 of the oxygen peaks for different RH as a function of the polarization state (up – upwards yellow filled triangles, down – downwards purple filled triangles, and up switched – upwards purple with blue line triangles): (b) the hydroxyl layer, corresponding to the purple peak of the spectra in (a), (c) the surface oxide species (green peak of spectra in (a)) and (d) the physisorbed molecular water (dark blue peak of the O 1s spectra).

observe that in agreement with the higher molecular water adsorption of the down-polarized surface, almost full electric discharge of this surface is achieved for a water pressure of 2 mbar (≈9% RH), while the trend for the up-polarized surface points to a complete discharge of the surface for 4 mbar (≈18.2% RH). In this sense, we can assume that for RH ≥ 20%, the water molecular coverage of the ferroelectric surface is high enough to ensure good surface electronic and ionic conductivity.

Overall, we can say that the hydroxylation state of the surface is determined by the water splitting potential of the as-grown polarization state of the surface but still, hydroxyl groups and water molecules seem to play a minor role as screening agents. Down-to-up polarization switching by the application of negative voltages to the surface clearly leads to: (i) the preservation of the hydroxylation state of the original sample, (ii) the enhancement of surface oxidized species and (iii) an enhancement of water affinity.

3.3. Charge dynamics on PZT thin film surfaces by PFM and KPFM

As schematically illustrated in Fig. 3, the application of a voltage *via* an SPM tip typically results in a highly localized concentration of surface charge, through either deposition or removal of charged species and/or electrochemistry. However, only when the SPM tip is biased appropriately and with sufficient strength – with positive voltages for up-polarized and negative voltages for down-polarized ferroelectric films – will polarization reversal actually occur. To probe all the different configurations and events, domain structures with switched (polarization reversed from its as-grown orientation) and charged (tip bias applied to generate an electric field aligned with the as-grown polarization orientation) regions, as well as an area scanned in contact with zero bias were created, as schematically illustrated in Fig. 3. Slightly different domain structures were used in the up-polarized and down-polarized samples.

KPFM can be used to study both spatial and temporal changes of the surface potential correlated to the presence of surface water,[6,57] giving evidence of the evolution of surface charged species over time (Fig. 3c and f). We qualitatively see two distinct trends of spatial distribution as a function of RH. First, at low humidity the edges of the areas scanned with a biased SPM tip are clearly visible, sharp and – most importantly – spatially confined to the region of writing (see Fig. S3†). This feature is very relevant in order to discriminate between ionic injected or mobile charges and fixed surface charges, or intrinsic surface potential values arising from the combination of ferroelectric polarization fields, screening charges and surface electrochemically induced species. When RH levels of 30–40% are reached, however, the surface potential contrast extends increasingly beyond the scanned areas and the KPFM signal is essentially passivated in as little as 15–45 minutes. We note that the KPFM signal at high RH is much more diffuse and extends outside the boundary of the written ferroelectric domain itself, which is determined independently *via* PFM to follow exactly the rectangular pattern imposed by the biased scanning tip (detailed in ESI†). These observations suggest that the increasing thickness of the surface water layer and water neck around the AFM tip modify the effective electric field distribution, enhancing the electrochemical effects, but that these modulations remain sub-coercive with respect to polarization switching.[58]

The KPFM signals from the switched up- and down-polarized areas compared to the as-grown back-ground region were averaged separately for each image, and extracted as a function of time. This yielded four independent data subsets: as-grown up-polarized sample reversed by positive voltage (resulting in a down-polarized state), as-grown up-polarized sample charged with negative voltage, as-grown down-polarized sample charged with positive voltage, and as-grown down-polarized sample reversed by negative voltage (resulting in an up-polarized state). A strongly nonlinear decay from the initial (positive or negative) signal level towards the background surface potential was observed in all cases (see Fig. S4†). A good description of this process is provided by a constrained dual exponential decay expression shown in eqn (1):

$$\begin{aligned} y_{\mathrm{sw}\pm}(t) &= y_{0\mathrm{sw}\pm} + A_{\mathrm{fast1}\pm}\exp(-t/\tau_{\mathrm{fast}\pm}) + A_{\mathrm{sw}\pm}\exp(-t/\tau_{\mathrm{sw}\pm}) \\ y_{\mathrm{ch}\pm}(t) &= y_{0\mathrm{ch}\pm} + A_{\mathrm{fast2}\pm}\exp(-t/\tau_{\mathrm{fast}\pm}) + A_{\mathrm{ch}\pm}\exp(-t/\tau_{\mathrm{ch}\pm}) \end{aligned} \quad (1)$$

where $y_{\mathrm{sw}\pm}(t)$ and $y_{\mathrm{ch}\pm}(t)$ are the KPFM signal intensities in the switched and charged areas as a function of the as-grown polarization state (+ for up polarized and − for down polarized), respectively, and $A_{\mathrm{sw}\pm}$, $A_{\mathrm{ch}\pm}$, $\tau_{\mathrm{sw}\pm}$ and $\tau_{\mathrm{ch}\pm}$ are the corresponding parameters of the decay. In this equation $y_{0\mathrm{sw}\pm}$ and $y_{0\mathrm{ch}\pm}$ denote permanent electrochemical changes produced on the surface by the application of a tip (constant during the 12 hours time frame of the experiment). This suggests the presence of two distinct mechanisms: a fast dynamics related to the actual dissipation/passivation of surface charge through the possible pathways along, through, or above the material, and a slower dynamics correlated with the electrochemistry at the surface of the ferroelectric thin film. The fits were constrained and optimized together for each applied voltage with a coupled time constant $\tau_{\mathrm{fast}\pm}$ for the fast sample-dependent decay, which has a polarity-dependent intensity $A_{\mathrm{fast1}\pm}$ or $A_{\mathrm{fast2}\pm}$. With these constraints, the fit performed simultaneously on all the data sets of surface potential decay for both positive and negative applied voltages as a function of humidity yielded excellent agreement, and a distribution of charge decay time constants, as shown in the ESI.†

The fast dynamics is dominated by the electronic and ionic conductivity, mainly through the surface.[9] Obtained τ_{fast} exponent takes values of $\tau_{\mathrm{fast}+}$ (as-grown up) = 280 ± 30 s for the up-polarized film and $\tau_{\mathrm{fast}-}$ (as-grown down) = 320 ± 65 s for the down-polarized film, and appears to be independent of humidity across the complete RH range (see Fig. S5a†). This value is in the same order of magnitude than previous reported relaxation times of 20 min for surface charges on $BaTiO_3$ single crystals[9] and similar to time constants of electronic/ionic diffusion on surface water layers, that are of order of 10^2 s on Si surface.[57] The time resolution of the our experiments is ≈1000 s due to the slow acquisition times of the images, so while they are still in agreement, unfortunately the absolute values of these time constants cannot be directly compared with time constants of electronic/ionic diffusion. Nevertheless, the lack of humidity dependence indicates that this fast process is a material characteristic behavior which we attribute to surface charge/ionic diffusion.

On the other hand, the remaining surface potential contrast dominated by the slow discharge dynamics once the mobile injected charges are released, has only three possible origins: (i) unscreened fields arising from bulk ferroelectric polarization (ii) different chemical composition of the sample close to the surface and (iii) chemisorbed ionic or charged species like dipoles created after redox reactions. While the first is an intrinsic sample effect associated to the ferroelectric polarization, the latter two highly depend on the electrochemistry caused by the SPM tip on the surface. Electrochemical reac-

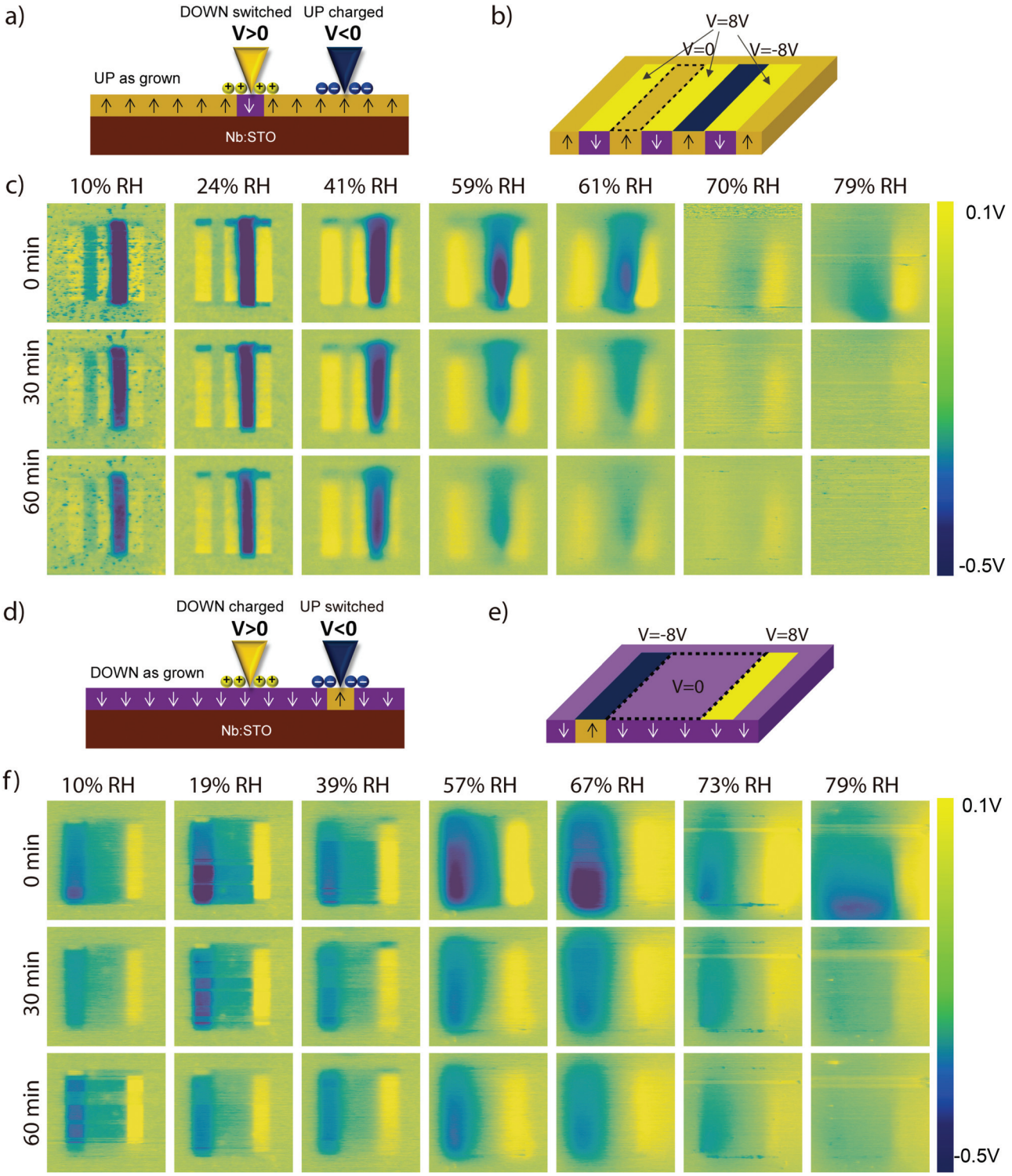

Fig. 3 Schematic representation of charge injection and polarization switching events for (a) an as-grown up-polarized and (d) as-grown down-polarized ferroelectric thin films. (b, e) Predetermined patterns for scanning tip bias application on the up- and down-polarized thin films, respectively. Corresponding KPFM images of the different areas with opposite applied electric fields a function of RH, and their evolution over time for the (c) as-grown up-polarized (f) and down-polarized thin films. KPFM images were mathematically flattened with respect to the background that is labelled to zero for all images on all surfaces (green colour) irrespective to the polarization orientation. The color scale ranges from +0.1 V to −0.5 V with respect to the back-ground surface potential (in green). Each images takes 15 minutes.

tions driven in water media at the surface will essentially lead to local oxidation and reduction of the surface oxide layer, but the nature of the cathodic and anodic half-reaction will strongly depend on the level of hydroxylation of the surface and the surface termination, for which the determination of the exact chemical reactions and involved ionic species is currently work under progress. Thus, the vanishing of KPFM contrast over long time scales can only be explained by (i) subsequent screening of the permanent new chemical species by media ionic charges or (ii) evolution of these created chemical species *via* continuous redox reactions at the interface between the ferroelectric and the water layer. Time constants of the slow dynamic processes $\tau_{sw\pm}$ and $\tau_{ch\pm}$ are shown in Fig. 4a, and take values of the order of 10^4 s, at the top limit of the time window of chemical reactivity and redox dynamics in water media and screening phenomena by dipolar molecules (typically in the order of tens of minutes). Still, their decrease with increasing RH suggests that the efficiency of these reactions at low RH might be limited and slowed down by the lack of reactants and active catalytic sites since our "liquid media" is in fact limited to a few monolayers. In all cases, oxidized species (symbols with blue outline) show faster relaxation times than reduced species (symbols with yellow outline).

The nature of electrochemical surface reactions can be further elucidated by comparing the permanent with the transient KPFM signals as shown in Fig. 4(b and c) as a function of the tip voltage: (i) the application of negative voltages ($V < 0$, blue lines) lead to more intense KPFM signals in both samples, indicating the higher efficiency of reduction reactions *vs.* oxidation reactions, (ii) the as-grown-down sample (purple triangles) shows major permanent changes in surface composition upon the application of voltages of both polarities and (iii) negative surface species created under the application of negative voltage (and probably reduction reactions) relax over time on up polarized surfaces (predominance of A_{ch+} in Fig. 4(c)), while they become permanent when they are associated with a ferroelectric polarization switching event (predominance of y_{0sw-} in Fig. 4(b)). We would expect but do not observe the corresponding behaviour of positive surface species under the effect of positive bias, but in this case we believe it is concealed by the error bars resulting from the weaker magnitude of the KPFM signal for this scenario.

It is no surprise that negative voltages applied to the SPM tip promote strong surface chemical reactions, and in fact, it is the reason why this configuration is not recommended for some electrical modes of SPM such as C-AFM. Second, looking back to the AP-XPS results, we can explain the higher degree of reactivity of the as-grown down-polarized sample by its higher initial degree of surface hydroxylation and water affinity as compared to the as-grown up-polarized sample. Moreover, we can correlate the permanent negative KPFM signal of the as-grown down-polarized sample upon the application of a negative voltage with the huge increase of the coverage of the O_{surf} species, suggesting that the enhanced retention of the surface potential corresponds to the presence of reduced species (or superoxide states) created after the tip-induced reduction reaction. Following observation (iii), we posit that these peroxide species may also have a relevant role in polarization screening for up polarized domains. Finally, the observed electrochemical reactions seem to fade away for RH > 70%. It is to be expected that the efficiency of tip induced electrochemical redox surface reactions decreases as water accumulates on the surface and/or there are more charges and ions available for screening.

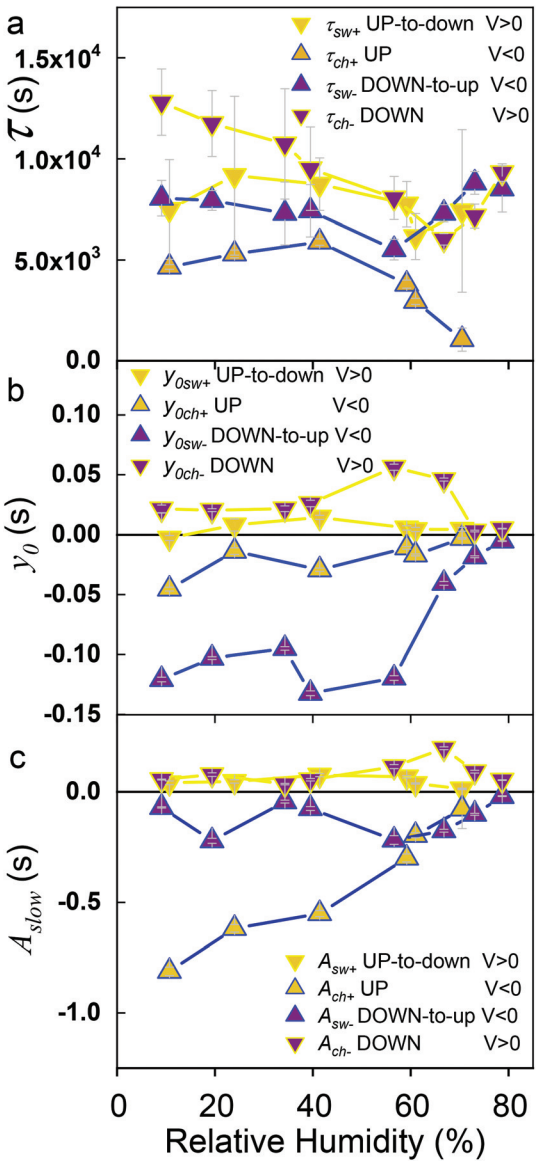

Fig. 4 Fitting parameters of eqn (1), for both surfaces (± up and down respectively) after charging and switching events: (a) slow time constants $\tau_{sw\pm}$ and $\tau_{ch\pm}$ (b) y_{0i} constants and (c) A_i slow decay amplitudes. The code for the symbols is as follows: up and down triangles indicate the final state of polarization respectively, the filling colours correspond to the initial state (dark yellow for as-grown up polarization and purple for as-grown down polarization) and the colour of the shape outline corresponds to the voltage applied to the tip (yellow for V = 8 V and blue for V = −8 V).

In summary, KPFM gives us insight into the nanoscale electrochemical reactions and their interaction with the locally

reversed ferroelectric polarization – the spatial extent of the observed KPFM signal highlights the key role of surface chemical species in charge retention and dissipation. The time evolution of the surface potential is clearly correlated with surface charging at the electronic and ionic level for the fast time scale. Instead, the presence of slow relaxation signal reveals the generation of transient redox species that stabilize on the surface in the time scale of hours. These redox species are more strongly fixed on the surface when they are created after a ferroelectric polarization switching event, probably due to their emerging role as screening agents. This is in agreement with the XPS measurements giving insight into the chemical composition of these surfaces, bridging the gap between the macro- and nanoscale understanding of humidity-dependent electrochemistry and charge dynamics on ferroelectric surfaces.

4. Conclusion

Our results clearly demonstrate that due to the electrochemical reactivity of ferroelectric materials, not only the relative humidity and polarization orientation, but also in a more complex fashion the *history* of charging/switching events determine the bulk and surface composition of ferroelectric thin films. The as-grown polarization state settles the initial ionic distribution of cations at the B sites of the perovskite structure close to the surface, as well as the composition of the surface adsorbates layer for PZT thin films. The ionic bulk distribution of Zr and Ti ions changes almost reversibly as a function of polarization state, showing an excess of Ti content close to the surface in down-polarized domains beyond its nominal bulk chemical ratio with respect to Zr. On the other hand, the surface chemical composition reveals itself as a footprint of the initial as-grown state of the sample, and reflects the polarization history. Furthermore, electrical switching of as-grown down domains by negative voltages into up polarization states, gives evidence of irreversible loss Pb as observed by XPS, pointing to a possible origin of ferroelectric fatigue. All in all, the configuration of PZT ferroelectric thin films and their surface adsorbates as a function of polarization direction can be summarized with the scheme in Fig. 5.

In addition, the application of voltage on a ferroelectric surface leads to permanent electrochemical changes the surface produced by redox reactions. Beyond eventual ferroelectric polarization switching events and/or mobile charge injection, high negative voltages applied to the oxide ferroelectric surfaces promote reduction reactions leading to surface peroxide species. These species give negative KPFM signal contrast, which vanishes over time when the surface is further reduced by interaction with environmental water molecules or becomes screened by other available ions or dipoles. When the peroxide species are created while switching the polarization, they additionally achieve a relevant role as surface screening agents that may slow down the redox rate, at least for RH < 70%, and they become almost permanent in the time scale of our experiments. When a positive voltage is applied to the ferroelectric surface, the most likely electrochemical reactions should be the oxidation of the surface oxide compounds, but these appear to be less efficient than reduction reactions, leading to weaker positive KPFM signals. The as-grown down-polarized surface shows higher reactivity under any applied voltage, presumably due to its higher initial hydroxylation state and stronger water affinity. Nonetheless in all cases, reduced species show faster relaxation times than oxidized species, and moreover, relaxation of redox species is slowed down to almost permanent in the time scale of our experiments when they play a role as screening agents.

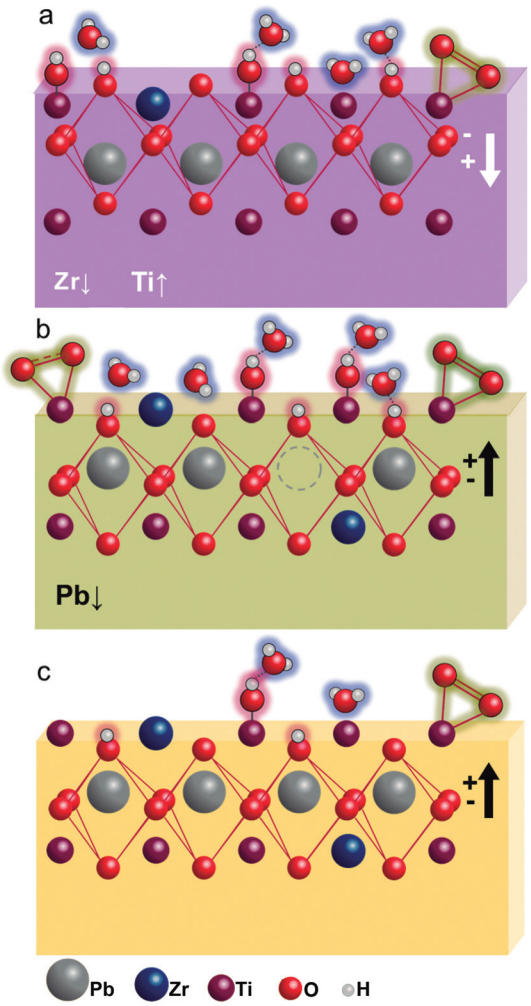

Fig. 5 Representative configuration of the surface stoichiometry and adsorbates on PZT ferroelectric thin films as a function of polarization direction: (a) as-grown down-polarized thin film, (b) down-to-up switched thin film after the application of $V = -8$ V and (c) as-grown down-polarized thin film. While the as-grown state creates a permanent footprint on the surface adsorbate arrangement, polarization switching correlates with internal, almost fully reversible electrochemical changes in the composition. In addition, the application of negative voltage to the surface produces oxidation reactions that lead to the appearance of surface peroxide species, with active roles as ferroelectric polarization screening agents.

In summary, we demonstrate that ferroelectricity and polarization switching are intrinsically entangled with electrochemical phenomena beyond screening mechanisms, both in bulk and at the surface, and especially those resulting from water-mediated electrochemical reactivity of ferroelectric surfaces. In particular, the surface chemical composition of adsorbates may play a weaker role than expected as a screening agent and instead, can be used as a characteristic footprint of the ferroelectric polarization history of PZT thin films.

Conflicts of interest

There are no conflicts to declare.

Acknowledgements

Financial support was obtained under projects from the Spanish Ministerio de Economía y Competitividad (MINECO) under projects FIS2015-73932-JIN and MAT2016-77852-C2-1-R (AEI/FEDER, UE), and by Division II of the Swiss National Science Foundation under project 200021_178782. ICN2 is supported by the Severo Ochoa program from Spanish MINECO (Grant No. SEV-2017-0706), and ICMAB acknowledges support from the Severo Ochoa Program (MINECO, Grant No. SEV-2015-0496). This work was partially funded by 2017-SGR-579 and 2017-SGR-668 projects from the Generalitat de Catalunya. The authors thank the support of ALBA staff for the successful performance of the measurements at CIRCE beamline from the ALBA Synchrotron Light Source.

References

1 S. V. Kalinin, Y. Kim, D. D. Fong and A. N. Morozovska, *Rep. Prog. Phys.*, 2018, **81**, 036502.
2 S. Hong, S. M. Nakhmanson and D. D. Fong, *Rep. Prog. Phys.*, 2016, **79**, 076501.
3 W. Yang, B. Rodriguez, A. Gruverman and R. Nemanich, *J. Phys.: Condens. Matter*, 2005, **17**, S1415–S1426.
4 C. Lichtensteiger, C. Weymann, S. Fernandez-Pena, P. Paruch and J.-M. Triscone, *New J. Phys.*, 2016, **18**, 043030.
5 I. Krug, N. Barrett, A. Petraru, A. Locatelli, T. O. Mentes, M. A. Nino, K. Rahmanizadeh, G. Bihlmayer and C. M. Schneider, *Appl. Phys. Lett.*, 2010, **97**, 222903.
6 J. J. Segura, N. Domingo, J. Fraxedas and A. Verdaguer, *J. Appl. Phys.*, 2013, **113**, 187213.
7 J. Shin, V. B. Nascimento, G. Geneste, J. Rundgren, E. W. Plummer, B. Dkhil, S. V. Kalinin and A. P. Baddorf, *Nano Lett.*, 2009, **9**, 3720–3725.
8 S. V. Kalinin and D. A. Bonnell, *Phys. Rev. B: Condens. Matter Mater. Phys.*, 2001, **63**, 125411.
9 S. V. Kalinin, C. Y. Johnson and D. A. Bonnell, *J. Appl. Phys.*, 2002, **91**, 3816–3823.
10 S. V. Kalinin and D. A. Bonnell, *Nano Lett.*, 2004, **4**, 555–560.
11 Y. Cao and S. V. Kalinin, *Phys. Rev. B*, 2016, **94**, 235444.
12 A. Kakekhani and S. Ismail-Beigi, *Phys. Chem. Chem. Phys.*, 2016, **18**, 19676–19695.
13 M. A. Khan, M. A. Nadeem and H. Idrissn, *Surf. Sci. Rep.*, 2016, **71**, 1–31.
14 N. Tyminska, G. Wu and M. Dupuis, *J. Phys. Chem. C*, 2017, **121**, 8378–8389.
15 N. Domingo, E. Pach, K. Cordero-Edwards, V. Pérez-Dieste, C. Escudero and A. Verdaguer, *Phys. Chem. Chem. Phys.*, 2019, **21**, 4920–4930.
16 K. Garrity, A. Kakekhani, A. Kolpak and S. Ismail-Beigi, *Phys. Rev. B: Condens. Matter Mater. Phys.*, 2013, **88**, 045401.
17 J. L. Wang, F. Gaillard, A. Pancotti, B. Gautier, G. Niu, B. Vilquin, V. Pillard, G. L. M. P. Rodrigues and N. Barrett, *J. Phys. Chem. C*, 2012, **116**, 21802–21809.
18 J. L. Wang, B. Vilquin and N. Barrett, *Appl. Phys. Lett.*, 2012, **101**, 092902.
19 J. H. Lee and A. Selloni, *Phys. Rev. Lett.*, 2014, **112**, 196102.
20 I. Grinberg, D. V. West, M. Torres, G. Gou, D. M. Stein, L. Wu, G. Chen, E. M. Gallo, A. R. Akbashev, P. K. Davies, J. E. Spanier and A. M. Rappe, *Nature*, 2013, **503**, 509.
21 S. M. Yang, A. N. Morozovska, R. Kumar, E. A. Eliseev, Y. Cao, L. Mazet, N. Balke, S. Jesse, R. K. Vasudevan, C. Dubourdieu and S. V. Kalinin, *Nat. Phys.*, 2017, **13**, 812–818.
22 C. Blaser and P. Paruch, *New J. Phys.*, 2015, **17**, 013002.
23 J. Y. Son, G. Lee and Y. H. Shin, *Appl. Phys. Lett.*, 2009, **94**, 162902.
24 A. V. Ievlev, S. Jesse, A. N. Morozovska, E. Strelcov, E. A. Eliseev, Y. V. Pershin, A. Kumar, V. Y. Shur and S. V. Kalinin, *Nat. Phys.*, 2014, **10**, 59–66.
25 H. Lee, T. H. Kim, J. J. Patzner, H. Lu, J.-W. Lee, H. Zhou, W. Chang, M. K. Mahanthappa, E. Y. Tsymbal, A. Gruverman and C.-B. Eom, *Nano Lett.*, 2016, **16**, 2400–2406.
26 M. J. Highland, T. T. Fister, D. D. Fong, P. H. Fuoss, C. Thompson, J. A. Eastman, S. K. Streiffer and G. B. Stephenson, *Phys. Rev. Lett.*, 2011, **107**, 187602.
27 Y. Cao, Q. Li, L.-Q. Chen and S. V. Kalinin, *Appl. Phys. Lett.*, 2015, **107**, 202905.
28 A. V. Ievlev, C. C. Brown, J. C. Agar, G. A. Velarde, L. W. Martin, A. Belianinov, P. Maksymovych, S. V. Kalinin and O. S. Ovchinnikove, *ACS Appl. Mater. Interfaces*, 2018, **10**, 38217–38222.
29 C. Barth, A. S. Foster, C. R. Henry and A. L. Shluger, *Adv. Mater.*, 2011, **23**, 477–501.
30 D. Y. He, L. J. Qiao and A. A. Volinsky, *J. Appl. Phys.*, 2011, **110**, 074104.
31 B. J. Rodriguez, S. Jesse, A. P. Baddorf and S. V. Kalinin, *Phys. Rev. Lett.*, 2006, **96**, 237602.
32 L. Collins, S. Jesse, J. I. Kilpatrick, A. Tselev, O. Varenyk, M. B. Okatan, S. A. L. Weber, A. Kumar, N. Balke, S. V. Kalinin and B. J. Rodriguez, *Nat. Commun.*, 2014, **5**, 3871.

33 S. Sanna, R. Hoelscher and W. G. Schmidt, *Phys. Rev. B: Condens. Matter Mater. Phys.*, 2012, **86**, 205407.
34 D. Y. He, L. J. Qiao, M. Khodayari and A. A. Volinsky, *J. Appl. Phys.*, 2014, **116**, 084105.
35 X. Li, B. Wang, T.-Y. Zhang and Y. Su, *J. Phys. Chem. C*, 2014, **118**, 15910–15918.
36 K. Cordero-Edwards, L. Rodriguez, A. Calo, M. J. Esplandiu, V. Perez-Dieste, C. Escudero, N. Domingo and A. Verdaguer, *J. Phys. Chem. C*, 2016, **120**, 24048–24055.
37 A. Verdaguer, C. Weis, G. Oncins, G. Ketteler, H. Bluhm and M. Salmeron, *Langmuir*, 2007, **23**, 9699–9703.
38 A. Belianinov, A. Ievlev, M. Lorenz, N. Borodinov, B. Doughty, S. Kalinin, F. Fernandez and O. Ovchinnikova, *ACS Nano*, 2018, **12**, 11798–11818.
39 S. M. Neumayer, A. V. Ievlev, L. Collins, R. Vasudevan, M. A. Baghban, O. Ovchinnikova, S. Jesse, K. Gallo, B. J. Rodriguez and S. V. Kalinin, *ACS Appl. Mater. Interfaces*, 2018, **10**, 29153–29160.
40 A. V. Ievlev, P. Maksymovych, M. Trassin, J. Seidel, R. Ramesh, S. V. Kalinin and O. S. Ovchinnikova, *ACS Appl. Mater. Interfaces*, 2016, **8**, 29588–29593.
41 S. V. Kalinin, S. Jesse, A. Tselev, A. P. Baddorf and N. Balke, *ACS Nano*, 2011, **5**, 5683–5691.
42 N. Balke, P. Maksymovych, S. Jesse, I. I. Kravchenko, Q. Li and S. V. Kalinin, *ACS Nano*, 2014, **8**, 10229–10236.
43 A. V. Ievlev, C. Brown, M. J. Burch, J. C. Agar, G. A. Velarde, L. W. Martin, P. Maksymovych, S. V. Kalinin and O. S. Ovchinnikova, *Anal. Chem.*, 2018, **90**, 3475–3481.
44 H. Lu, C. W. Bark, D. Esque de los Ojos, J. Alcala, C. B. Eom, G. Catalan and A. Gruverman, *Science*, 2012, **336**, 59–61.
45 H. Lu, S. Liu, Z. Ye, S. Yasui, H. Funakubo, A. M. Rappe and A. Gruverman, *Appl. Phys. Lett.*, 2017, **110**, 222903.
46 J. Ocenasek, H. Lu, C. W. Bark, C. B. Eom, J. Alcala, G. Catalan and A. Gruverman, *Phys. Rev. B: Condens. Matter Mater. Phys.*, 2015, **92**, 035417.
47 H. Bluhm, *J. Electron Spectrosc. Relat. Phenom.*, 2010, **177**, 71–84.
48 D. E. Starr, Z. Liu, M. Haevecker, A. Knop-Gericke and H. Bluhm, *Chem. Soc. Rev.*, 2013, **42**, 5833–5857.
49 I. Gaponenko, L. Gamperle, K. Herberg, S. C. Muller and P. Paruch, *Rev. Sci. Instrum.*, 2016, **87**, 063709.
50 S. Gariglio, N. Stucki and J.-M. Triscone, *Appl. Phys. Lett.*, 2007, **90**, 202905.
51 V. Pérez-Dieste, L. Aballe, S. Ferrer, J. Nicolàs, C. Escudero, A. Milán and E. Pellegrin, *J. Phys.: Conf. Ser.*, 2013, **425**, 072023.
52 N. Apostol, *AIP Conf. Proc.*, 2014, **1634**, 81–88.
53 N. Domingo, N. Bagues, J. Santiso and G. Catalan, *Phys. Rev. B: Condens. Matter Mater. Phys.*, 2015, **91**, 094111.
54 Y. Yun and E. I. Altman, *J. Am. Chem. Soc.*, 2007, **129**, 15684–15689.
55 G. Ketteler, S. Yamamoto, H. Bluhm, K. Andersson, D. E. Starr, D. F. Ogletree, H. Ogasawara, A. Nilsson and M. Salmeron, *J. Phys. Chem. C*, 2007, **111**, 8278–8282.
56 A. Verdaguer, J. J. Segura, J. Fraxedas, H. Bluhm and M. Salmeron, *J. Phys. Chem. C*, 2008, **112**, 16898–16901.
57 A. Verdaguer, M. Cardellach, J. J. Segura, G. M. Sacha, J. Moser, M. Zdrojek, A. Bachtold and J. Fraxedas, *Appl. Phys. Lett.*, 2009, **94**, 233105.
58 A. BrugÃĺre, S. Gidon and B. Gautier, *J. Appl. Phys.*, 2011, **110**, 052016.